PREDICTING LONG-TERM PERCOLATION FROM THE HTF AND FTF CLOSURE CAPS

Sarah A. Gustitus and Craig H. Benson

Report No. GENV-20-09

University of Virginia/CRESP
Charlottesville, VA 22904 USA

24 June 2020

EXECUTIVE SUMMARY

The objective of this study was to provide updated predictions of the percolation rate emanating from the base of the engineered closure cap (herein “ECC”) anticipated for closure of H-Area Tank Farm (HTF) and F-Area Tank Farm (FTF) at the Savannah River Site (SRS). The ECC is a multilayer final cover employing a composite barrier system and an earthen lateral drain as the primary features that control flow of meteoric water. Hydrology of the ECC was predicted using a coupled model based on the most recent information available regarding the engineering properties of final covers. The variably saturated flow code WinUNSAT-H was used to predict unsaturated flow, atmospheric interactions, and deep drainage for the portion of the cover profile overlying the lateral drainage layer. A combination of analytical and semi-analytical equations was used to predict flow in the drainage layer and percolation from the base of the composite barrier using the deep drainage predicted by WinUNSAT-H as input.

Simulations were conducted with meteorological conditions representing wet conditions in the current climate and two climate change scenarios corresponding to wet and very wet conditions. Predictions were made for conditions where the drainage layer and composite barrier continue to function as intended, and where degradation of the drainage layer and composite barrier occur due to clogging of the drainage layer, oxidation of the geomembrane, or severe gully erosion that penetrates down to the composite barrier. For many scenarios, very low percolation rates (<1 mm/yr) are predicted even if climate change occurs that imposes very wet conditions and the geomembrane undergoes degradation due to long-term oxidation. These low percolation rates are contingent on the drainage layer remaining permeable, the GCL retaining low hydraulic conductivity, and the erosion barrier preventing severe gully erosion. These conditions are consistent with near-term (<20 yr) experience with in-service final covers as well as historic natural analogs, and are considered the most plausible. Higher percolation rates are predicted if the drainage layer becomes much less permeable, the GCL becomes more permeable, or severe gully erosion occurs that damages the composite barrier. Long-term percolation rates on the order of 50 mm/yr can occur if the drainage layer becomes less permeable and stress cracks form in the geomembrane. In the most severe case, percolation rates on the order of 170 mm/yr are possible if severe gully erosion occurs. These higher percolation rates ($\geq$ 50 mm/yr) are plausible, but unlikely.

TABLE OF CONTENTS

LIST OF TABLES AND FIGURES

1. INTRODUCTION

The objective of this study was to use the latest available information to provide predictions of percolation rates from the bottom of the engineered closure caps (herein "ECC") anticipated for closure of the H-Area Tank Farm (HTF) and F-Area Tank Farm (FTF) at the Savannah River Site (SRS). These percolation rates will be used by others in predictive models as part of performance assessments (PA) for the HTF and FTF. The predictions described in this report are based on the most recent information available regarding the engineering properties of final covers derived from the US Environmental Protection Agency's (USEPA) Alternative Cover Assessment Program (ACAP), the US Nuclear Regulatory Commission's (NRC) evaluation of engineered covers for waste containment (NUREG CR-7028, Benson et al. 2011), and research conducted by the US Department of Energy's Consortium for Risk Evaluation with Stakeholder Participation (CRESP) (Benson et al. 2010, Scalia et al. 2011, 2017, Tian et al. 2016, 2017, 2018). This information reflects the current state-of-the-art for final covers for waste containment systems and is based on 25 years of research and development.

The ECC is a multilayer final cover employing a composite barrier system and a sand lateral drain as the primary features that control flow of meteoric water into the underlying waste. A schematic of the cover is shown in Fig. 1. The composite barrier system consists of a geosynthetic clay liner (GCL) overlain by a geomembrane and a nonwoven geotextile, the latter intended to provide protection against puncture. The lateral drainage layer is directly above the geotextile and will be constructed from processed sands generated locally. The composite barrier and drainage layer are overlain by a geotextile, middle backfill layer 305 mm thick, an erosion barrier 305 mm thick, an upper backfill layer 760 mm thick, and a top soil layer 150 mm thick. The upper top soil has native species as vegetation that will root into the upper backfill layer.

Hydrology of the ECC is affected primarily by infiltration into the surface of the cover that becomes deep drainage through the backfill layers. This deep drainage impinges on the upper

lateral drainage layer (henceforth referred to as the drainage layer) and moves laterally on the upper surface of the composite barrier. Some of the water in the drainage layer contacts defects in the geomembrane, and becomes percolation (*aka* "leakage") from the composite barrier. This percolation will migrate downward, spreading laterally, and ultimately contacting the underlying waste. The primary objective of this study was to predict the percolation rate from the composite barrier over time using the best available information for different possible scenarios.

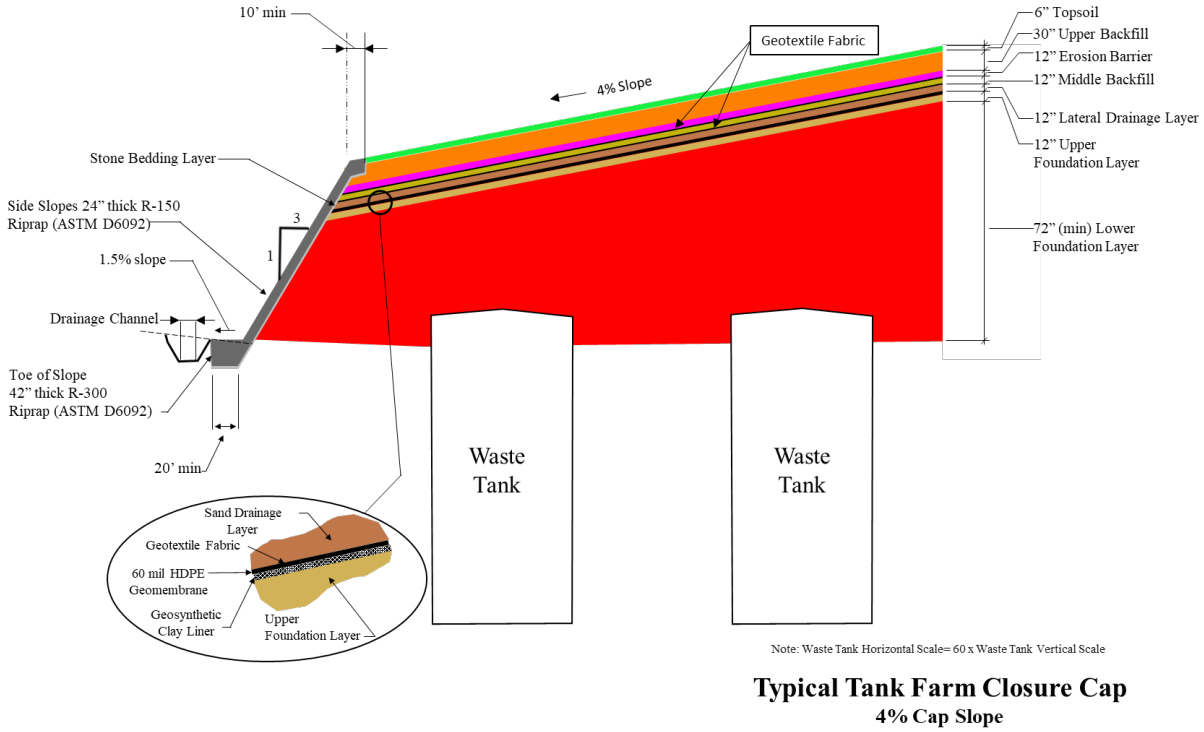

Fig. 1. Schematic of ECC planned for the HTF and FTF.

2. METHODOLOGY

Hydrology and percolation from the base of the ECC for the HTF and FTF were predicted using a coupled model that combines state-of-the-art techniques to simulate variably saturated flow in multilayer engineered covers with resistive barrier layers. The model was parameterized

with the most current and reliable information on the hydraulic properties of cover soils and the service life of geosynthetic layers.

A conceptual illustration of the coupled model is shown in Fig. 2. The model is composed of two components: (i) a variably saturated flow program (WinUNSAT-H) to predict unsaturated flow, water redistribution, and atmospheric interactions for the portion of the cover profile overlying the drainage layer and (ii) a combination of analytical and semi-analytical equations used to predict flow in the drainage layer and percolation from the base of the composite barrier.

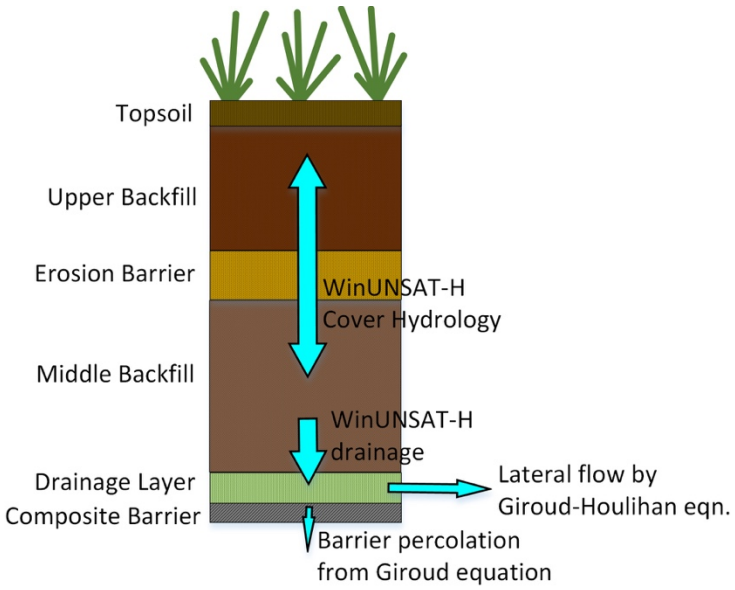

Fig. 2. Conceptual illustration showing components of coupled model used to predict percolation from base of ECC.

2.1 Variably Saturated Flow Model

WinUNSAT-H was used to predict variably saturated flow and atmospheric interactions above the drainage layer (Benson et al. 2004, Benson 2010). WinUNSAT-H is the Windows® implementation of the UNSAT-H code (Fayer et al. 1992, Fayer and Gee 1997) developed to predict variably saturated flow at the Hanford site and to design the Hanford Barrier. WinUNSAT-H has been used extensively over the past two decades for predicting the hydrology of covers for

waste containment systems, and is the most widely used model for design of water balance final covers. WinUNSAT-H has been used for a diverse range of climates, and has been verified using data sets from large-scale field experiments in USEPA's ACAP and other field-scale studies (Fayer and Gee 1997, Khire et al. 1997, 1999; Scanlon et al. 2002, Ogorzalek et al. 2008, Bohnhoff et al. 2009). Deep drainage from the base of the middle backfill layer (Fig. 2) predicted by WinUNSAT-H was used as the impingement rate (q) to the lateral drainage layer.

WinUNSAT-H solves a modified form of Richards' equation:

$$\frac{\partial\theta}{\partial\psi}\frac{\partial\psi}{\partial t} = -\left[K_c\frac{\partial\psi}{\partial z} + K_\psi\right] - S(z,t) \quad (1)$$

where θ = volumetric water content, ψ = matric suction, t = time, z = depth below ground surface (z=0 at the ground surface), K_ψ = unsaturated hydraulic conductivity, K_c = a combined hydraulic conductivity accounting for liquid and vapor flows, and S(z,t) = a sink term for root water uptake. WinUNSAT-H is a one-dimensional model that employs the finite-difference method to solve Eq. 1. Two-dimensional simulations were considered unnecessary because of the shallow slope (≤4.7%) of the cover. Isothermal simulations were conducted.

WinUNSAT-H employs an atmospheric boundary condition consisting of evaporation or infiltration, with runoff computed as the difference between applied precipitation and infiltration. Infiltration rate is controlled by the rate at which precipitation is applied and by the infiltration capacity of the cover, the latter defined by the hydrologic conditions in the cover during infiltration. Evaporation is computed as the liquid flux at the surface boundary using Darcy's Law, and is bounded by the potential evaporation (PE) rate (Fayer 2000). Several boundary conditions can be applied at the lower boundary. In this study, a unit gradient boundary was used to simulate deep drainage from the base of the middle backfill layer into the drainage layer.

WinUNSAT-H simulates vegetative water uptake using a mechanistic approach where potential transpiration (PT) is distributed throughout the root zone in proportion to the relative root density. PT and PE are computed from potential evapotranspiration (PET) based on the leaf area

index using the Ritchie-Burnett-Ankeny equation described in Chadwick et al. (1999), with PET computed using the modified Penman equation in Doorenbos and Pruitt (1977). Constraints on evaporation due to water availability are simulated using the plant limiting function in Feddes and Zaradny (1978), which is defined by the anaerobiosis point, limiting point, and wilting point (Bohnhoff et al. 2009). Root water uptake at a given depth ceases when the suction exceeds the wilting point or is below the anaerobiosis point.

Spatial and temporal discretization were adjusted to achieve a mass balance error < 1 mm/yr. The nodal spacing or element thickness was 1 mm near the boundaries and as large as 60 mm away from the boundaries. The maximum time step was 0.25 h and the minimum time step was $1x10^{-5}$ h. WinUNSAT-H automatically adjusts between these bounds, with small time steps used to ensure accuracy during periods of more rapid change and larger time steps to expedite computation during periods of lesser change. Simulations were performed on a laptop computer running the Windows® 10 operating system using a single processor. These relatively stringent control parameters resulted in simulation times of up to one hour.

2.2 Percolation from Composite Barrier

Analytical models were used to predict the percolation rate from the base of the composite barrier using deep drainage predicted by WinUNSAT-H as the impingement rate (q) on the drainage layer. The geomembrane in the composite barrier was assumed to contain circular defects, long rectangular defects, or both depending on the scenario being considered. Regardless of defect type, the Giroud-Houlihan analytical solution, which is based on Darcy's Law and mass balance principles (Giroud et al. 2004), was used to determine the head on the composite barrier (d) based on flow in the lateral drainage layer:

$$d = \frac{q\,L}{K_d \tan\beta} \tag{2}$$

where L is the length of run of the drainage layer, β is the slope angle for the drainage layer, and K_d is the saturated hydraulic conductivity of the drainage layer.

2.2.1 Circular Holes in Geomembrane

The leakage rate (Q) from a single circular defect in the composite barrier was computed using the formulation in Giroud et al. (1997):

$$Q = C\left[1+\frac{1}{10}\left(\frac{d}{t_g}\right)^{0.95}\right]a^{0.1}d^{0.9}K_s^{0.74} \tag{3}$$

where C is a contact factor for a circular or square defect, t_g is the thickness of the composite barrier (geomembrane and GCL), a is area of an average defect, and K_s is the saturated hydraulic conductivity of the GCL. Foose et al. (2001) have shown that Eq. 3 tends to over-estimate the leakage rate modestly, even when the lower bound for the contact factor ("good contact" condition, Giroud 1997) is used in analysis.

The percolation rate (P) from the composite barrier for circular defects is computed by combining Eqs. 2 and 3 and considering the number of circular defects in the composite barrier per unit surface area (N_d):

$$P=N_dC\left[1+\frac{1}{10}\left(\frac{qL}{t_gK_d\tan\beta}\right)^{0.95}\right]a^{0.1}\left(\frac{qL}{K_d\tan\beta}\right)^{0.9}K_s^{0.74} \tag{4}$$

Lateral spreading away from the defect and over the area of the cover is assumed to occur as the percolation penetrates downward beneath the cover.

2.2.2 Stress Cracks

The leakage rate for the composite barrier with a single rectangular defect (e.g., a stress crack) in the geomembrane was computed using (Giroud 1997):

$$Q=C\left[1+\frac{1}{10}\left(\frac{d}{t_g}\right)^{0.95}\right]b^{0.2}d^{0.9}K_s^{0.74}+C_\infty\left[1+\frac{1}{5}\left(\frac{d}{t_g}\right)^{0.95}\right](B\text{-}b)b^{0.1}d^{0.45}K_s^{0.87} \quad (5)$$

where B is the length of the defect, b is the width of the defect, and C_∞ is a contact factor for a defect of infinite length. Eqs. 2 and 5 can be combined to calculate percolation rate for a composite barrier with N_c stress cracks in the geomembrane:

$$P=N_cC\left[1+\frac{1}{10}\left(\frac{qL}{t_gK_d\tan\beta}\right)^{0.95}\right]b^{0.2}\left(\frac{qL}{K_d\tan\beta}\right)^{0.9}K_s^{0.74} +N_cC_\infty\left[1+\frac{1}{5}\left(\frac{qL}{t_gK_d\tan\beta}\right)^{0.95}\right](B\text{-}b)b^{0.1}\left(\frac{qL}{K_d\tan\beta}\right)^{0.45}K_s^{0.87} \quad (6)$$

2.3 Erosion Gullies

Scenarios were considered where gullies had formed due to erosion of part or all of the earthen components of the cover above the composite barrier. Gully widths for these scenarios were computed using the methodology in Sidorchuk (1999), where the width of the base of the gully (W_b) is defined based on the flow rate (Q_g) defining the width of flow forming the gully:

$$W_b = 60\ Q_g^{0.4} \quad (7)$$

where W_b is in m and Q_g is in m^3/s. Flow rates input to Eq. 7 were obtained from daily runoff predictions from WinUNSAT-H.

3. MODEL INPUT

Input to the model generally followed the methodology described in Benson and Benavides (2018) for the ECC over the Saltstone Disposal Facility (SDF), with adaptations made for additional scenarios considered in this analysis and new information.

3.1 Meteorological Conditions

WinUNSAT-H requires daily inputs of precipitation, maximum and minimum air temperature, relative humidity, wind speed, and solar radiation. Meteorological data from Jones and Phifer (2008) supplemented with more recent on-site data and solar radiation data from NASA's MERRA-2 database were used as input to WinUNSAT-H. The on-site data were obtained from monitoring point 700-A, which had the most complete data set for the entire range. Solar radiation data were obtained from NASA's MERRA-2 database for nearby Aiken, SC (Gelaro et al. 2017). MERRA-2 was chosen as the source of solar radiation data because a complete data set spanning the period of interest was available. The combined data set spans 1964 to 2016.

Annual precipitation in the record is shown vs. time in Fig. 3. Annual precipitation during the period 1964 to 2016 ranges from 724 to 1830 mm, with an average of 1196 mm. Of the 53 years in the data set, 32 years (60.4%) fall at or below average cumulative precipitation, and 21 years (39.6%) have above average precipitation. Only three years exceed the 95^{th} percentile (1650 mm): 1964, 1971, and 2003.

Two periods in the data set were selected for use in analysis: a "typical year" and the wettest 10-year period, as described in Benson and Bareither (2012). Simulations conducted with the "typical year" represent current average conditions. Simulations conducted with the wettest 10-yr period represent a wetter state under current climate conditions. Walsh et al. (2014) indicate that an increase in annual precipitation on the order of 5 to 10% can be anticipated in the region near SRS over the years 2070-2100 due to climate change. This increase in precipitation will also be accompanied by an increase in average temperature and a reduction in the frequency of sub-

freezing conditions (Carter et al. 2014). Greater precipitation and higher temperatures promote additional biomass growth, longer growing seasons, and higher evapotranspiration (ET) (Allen et al. 1998). Elevated ET from these factors reduces deep drainage. Thus, the elevated precipitation simulations represent a wet long-term scenario.

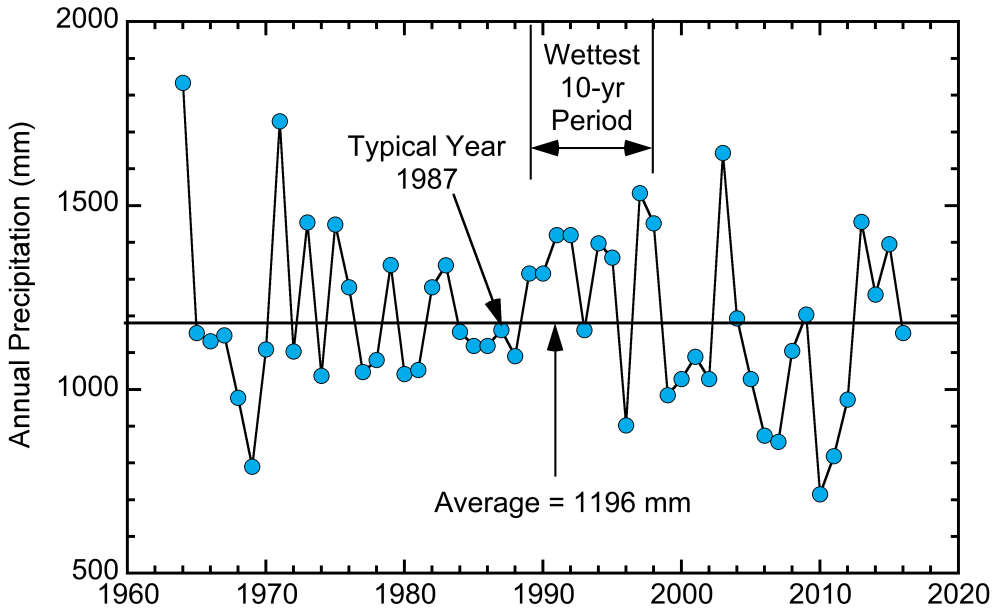

Fig. 3. Annual precipitation record from 1964 to 2016.

The “typical year” was selected from the dataset following the approach in Benson and Bareither (2012) and Bareither et al. (2015) as a year without highly unusual meteorological events that has annual precipitation close to the average annual precipitation (1987 with 1163 mm of precipitation). Typical years are different from long-term average conditions because a typical year is an actual data set that exhibits natural variability, and is not affected by the smoothing inherent in long-term averages. The wettest 10-yr period was selected using a moving average to determine which 10-yr period has the highest average annual precipitation. The wettest 10-yr period is 1989-1998, which is shown in Fig. 4. During this period, the site received 13,300 mm of precipitation (1330 mm/yr, or 11.2% above average annual precipitation). Annual precipitation was above the long-term average precipitation for 8 of the 10 years of the wettest

10-yr period. Electronic resources associated with this report contain the meteorological data sets for the average year and wettest 10-yr period.

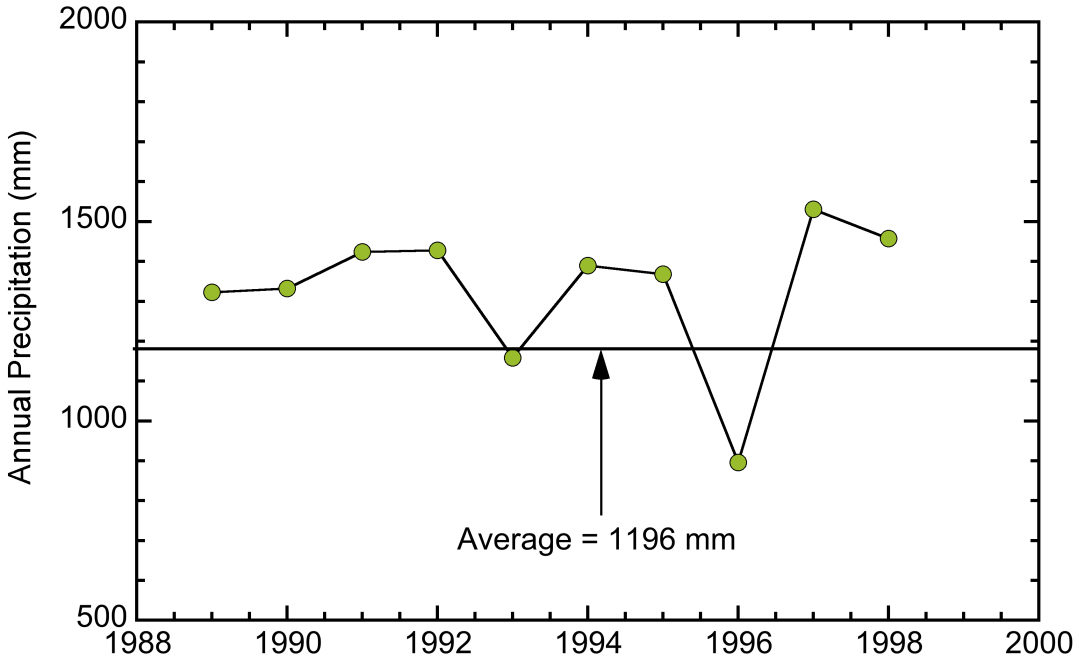

Fig. 4. Annual precipitation record for wettest 10-yr period.

3.2 Vegetation

Vegetation on the cover was assumed to be natural perennial grass cover during the institutional control period (100 yr), as exists at other locations at SRS and at the adjacent Barnwell disposal facility. Ingress of pine has been postulated over the long term, and planting of bamboo at the end of the institutional control period has been proffered to preclude ingress of pine (Jones and Phifer 2008). Transpiration characteristics of both species are difficult to quantify and input into a variably saturated flow model. However, both species will transpire more than a grass. The bamboo has greater leaf area, and transpiration is proportional to leaf area (e.g., Chadwick et al. 1999). Pine transpires year round and enhances interception, resulting in greater

transpiration. Thus, assuming grass cover results in higher predictions of deep drainage entering the lateral drainage layer compared to pine or bamboo cover.

Attributes of the natural perennial grass cover were characterized using data from field sites with natural grass cover in Atlanta, Georgia and Albany, Georgia. Both of these sites are in proximity to the Savannah River Site, and are associated with large-scale field tests to evaluate the hydrologic performance of covers for waste containment (Khire et al. 1997, Roesler et al. 2002, Albright et al. 2004, 2006, 2010, Apiwantragoon et al. 2014). The maximum root depth was set at the depth of the erosion barrier (Figs. 1, 2) and the root growth rate was set at 3 mm/d as recommended in Roesler et al. (2002). Root length densities (R_d) were described using the exponential function:

$$R = a\, e^{-zb} + c \tag{8}$$

where z is depth (m) and a = 0.44, b = 8.0 m^{-1}, and c = 0.055 based on data in Khire et al. (1997) and Roesler et al. (2002). Start of the growing season was set at Julian day 45 and end of the growing season was set at Julian day 345 based on Khire et al. (1997) and Roesler et al. (2002). Coverage was assumed to be 75% based on information in Roesler et al. (2002). The wilting point was set at 1500 kPa, the limiting point at 100 kPa, and the anaerobiosis point at 5 kPa based on information in Khire et al. (1997) and Roesler et al. (2002). Leaf area index (LAI) was assigned using the linear model shown in Fig. 5 following the method in Bohnhoff et al. (2009) using information from Khire et al. (1997) and Roesler et al. (2002). The peak LAI in Fig. 5 is 2.0, which is lower than would be expected with bamboo cover (Zhaoming et al. 2011) and similar to that expected for a pine cover (López-Serrano et al. 2000).

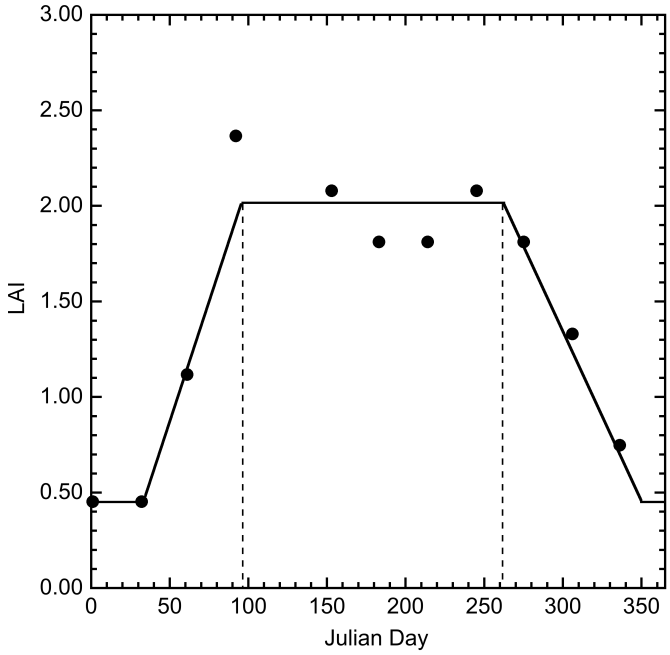

Fig. 5. Linear LAI function used as input to WinUNSAT-H.

3.3 Initial Conditions

Realistic initial conditions for the simulations were created by running a 5-yr simulation with WinUNSAT-H using the meteorological record for the typical year as input for each year, assuming an initial matric head of 100 kPa throughout the profile for the first day of the first year. Heads from day 30 from the end of the 5-yr simulation were used as the initial conditions for the wettest 10-yr period. Heads from the end of the year were unseasonably dry; therefore, day 30 heads were chosen as an early point in the year with reasonably low head, corresponding to wet conditions common in winter. This approach provides a realistic yet conservative initial condition that reflects hydrologic processes occurring within the cover profile.

3.4 Hydraulic Properties

WinUNSAT-H requires the saturated hydraulic conductivity (K_s), soil water characteristic curve (SWCC) parameters, and the pore interaction term in the unsaturated hydraulic conductivity

function as input to describe the unsaturated and saturated hydraulic properties of the cover soils. The SWCC was assumed to follow the van Genuchten equation (van Genuchten 1980):

$$\theta = \theta_r + \left(\theta_s - \theta_r\right)\left[\frac{1}{1+(\alpha\psi)^n}\right]^m \tag{9}$$

where θ is the volumetric water content, θ_s is the saturated volumetric water content, θ_r is the residual volumetric water content, α and n are shape parameters that describe the rate at which the water content changes with matric potential (ψ), and m = 1-n^{-1}. The unsaturated hydraulic conductivity (K_θ) function was assumed to follow the van Genuchten-Mualem model:

$$K_\theta = K_s \Theta^\ell \left[1-(1-\Theta^{1/m})^m\right]^2 \tag{10}$$

where ℓ is the pore interaction term and Θ is the effective saturation:

$$\Theta = \frac{\theta - \theta_r}{\theta_s - \theta_r} \tag{11}$$

The pore interaction term in Eq. 10 was assumed to be -1.5 for all soils in the cover profile, which is in the range for fine-textured soils described in Bohnhoff et al. (2009), Albright et al. (2010), and Benson (2010) for modeling the hydrology of earthen covers. Examples of how α, n, and ℓ affect the shape of the SWCC, the unsaturated hydraulic conductivity function, and hydrologic predictions can be found in Bohnhoff et al. (2009) and Benson (2006, 2010).

3.4.1 Topsoil

The topsoil layer will be sourced on site and will generally be sandy loam to loamy sand. Properties of the top soil that were assumed are summarized in Table 1. They are the same properties originally used in Jones and Phifer (2008) and are consistent with those in Benson et

al. (2007) for surface layers on covers that have undergone pedogenesis. As shown subsequently, the topsoil was sufficiently permeable to maintain runoff < 15% of the total annual water balance, as recommended by Albright et al. (2010) for hydrologic modeling of covers.

3.4.2 Upper and Middle Backfill Layers

The upper and middle backfill layers will be composed of clayey sands from borrow sources on-site and are similar to those encountered in nearby field studies of final covers reported in Khire et al. (1997), Albright et al. (2004, 2006), and Apiwantragoon et al. (2014). Properties of the upper and middle backfill layers were assumed to be the same and are summarized in Table 1. The saturated hydraulic conductivity (K_s) and the van Genuchten α parameter are consistent with and near the upper bound of the NRC recommendations on hydraulic properties for earthen covers in NUREG CR-7028 (Benson et al. 2011). These properties are recommended in NUREG CR-7028 (Benson et al. 2011) for simulating long-term naturalized conditions in performance assessments. They represent soils that have undergone pedogenesis and are in equilibrium with their surroundings.

Table 1. Hydraulic properties of earthen layers in ECC.

Layer	Saturated Hydraulic Conductivity, K_s (m/s)	Saturated Volumetric Water Content θ_s (-)	α (1/kPa)	n (-)
Topsoil	$3x10^{-5}$	0.40	0.17	1.3
Upper Backfill	$5x10^{-7}$	0.40	0.02	1.3
Erosion Barrier	$5x10^{-7}$	0.15	0.02	1.3
Middle Backfill	$5x10^{-7}$	0.40	0.02	1.3

Note: residual water content, θ_r, set to zero for all soils.

3.4.3 Erosion Barrier

The erosion barrier will be composed of angular stone sourced from a local quarry. The pore space in this layer will be infilled with sandy material, fine textured soil similar to the adjacent

backfill layers, or grout. For this analysis, the infill was assumed to be fine-textured soil having the same properties as the upper and lower backfill layers, but with the saturated water content reduced to account for the porosity of the stone using the method in Bareither and Benson (2013). This assumption eliminates a capillary break between the upper backfill and the erosion barrier, which would retain water more closely at the surface. Of the infill options, fine-textured infill maximizes flow of water into the underlying lower backfill.

3.4.4 Upper Lateral Drainage Layer

The drainage layer is expected to be a clean and relatively uniformly graded coarse sand. Water flowing downward through the middle backfill layer will enter the upper surface of the drainage layer, and then move laterally due to the presence of the geomembrane. The lateral drainage layer was not included in the WinUNSAT-H simulations, which eliminated any resistance to flow that might be afforded by the capillary break that will form between the fine-textured middle backfill layer and the coarse-grained drainage layer. Because this capillary break was not included, deep drainage for the middle backfill layer predicted by WinUNSAT-H should be greater than the actual rate at which water would impinge on the drainage layer in the field.

Saturated hydraulic conductivity is the only engineering property of the drainage layer that affects the percolation rate computed with Eqs. 4 and 6, in addition to geometric conditions (slope angle, drain length). For this study, saturated hydraulic conductivity was assumed to be $5x10^{-4}$ m/s, $1x10^{-4}$ m/s, or $1x10^{-5}$ m/s depending on the condition being evaluated. This range of hydraulic conductivities is consistent with those assumed in Jones and Phifer (2008), and captures realistic conditions, unlikely conditions (<5% chance of occurrence), and highly unlikely conditions (<1% chance of occurrence). The lower bound of $1x10^{-5}$ m/s is highly unlikely. Jones and Phifer (2008) assumed that the hydraulic conductivity of the drainage layer diminished over time from $5x10^{-4}$ to $1x10^{-5}$ m/s due to infilling of fines from the overlying backfill layer, a phenomenon that has not

observed during exhumation of modern final covers or in historic sites that are analogs (Benson and Benavides 2018).

The engineering design incorporates a geotextile filter between the upper surface of the drainage layer and the lower surface of the middle backfill layer. The geotextile is a nonwoven polymeric material buried at depth that is shielded from ultraviolet radiation and in an environment where oxidation is highly constrained. The service life of the geotextile likely will be as long as the geomembrane (~2000 yr, see subsequent discussion), and certainly will be several hundred years. However, even if the geotextile degraded completely, the filtration function would remain. A natural filter layer composed of fine particles develops on the upper surface of a geotextile used for filtration. This natural filter layer prevents migration of fines in a layered system (Koerner 2005), and will continue to be effective even if the geotextile degraded and was no longer present.

Even without a geotextile, near-term and historic analogs illustrate that fine-over-coarse interfaces at depth are stable over very long periods of time (Benson and Benavides 2018). A near-term example is illustrated in NUREG CR-7028 (Benson et al. 2011) and historical analogs are described in Bjornstad and Teel (1993), Onitsuka et al. (2003), and Hudson and Barnes (1991). Therefore, there is no reason to assume that the hydraulic conductivity of the drainage layer in the ECC will diminish over time.

3.4.5 Composite Barrier

The composite barrier layer consists of a high density polyethylene (HDPE) geomembrane over a geosynthetic clay liner (GCL) and is the primary barrier to percolation in the ECC. The geomembrane is impervious when intact. Even with extensive quality assurance, however, some defects in the geomembrane are inevitable and provide a point where water can flow through the barrier. The GCL beneath the geomembrane provides resistance to flow at defects, controlling flow through the barrier system. In effect, the geomembrane and GCL work together as a system with the geomembrane controlling the area over which flow occurs and the GCL controlling the

rate of flow in areas where geomembrane defects present. For this reason, the combination of a geomembrane and GCL is referred to as a composite barrier (Benson 2001). As indicated in Eqs. 4 and 6, the number and size of defects in the geomembrane along with the saturated hydraulic conductivity of the GCL are the engineering properties of the barrier layer that affect the percolation rate.

The geomembrane was assumed to contain only circular defects prior to antioxidant depletion and oxidation (<1000 yr; Tian et al. 2017, 2018). After antioxidation depletion and initiation of oxidation (>1000 yr; Tian et al. 2017, 2018), the geomembrane was assumed to contain larger circular defects and, in certain scenarios, long rectangular defects representing stress cracks when the stress crack resistance was depleted. For both cases, the geomembrane was assumed to have five circular defects per hectare, which is consistent with a high level of quality control reported by several case studies (Giroud and Bonaparte 1989). This estimate should be conservative since geomembrane installation practices have improved significantly since 1989. Each defect was assumed to be either 2 mm or 10 mm in diameter, depending on the analysis being conducted. A hole diameter of 10 mm is used in practice to size collection and monitoring systems for maximum flows, whereas 2 mm is recommended for predicting performance (Giroud and Bonaparte 1989). The number of defects was assumed to be constant for all simulations, as the most recent evidence indicates that the service life of HDPE geomembranes in low-level radioactive waste facilities is in excess of 1900 years, even in environments where the waste to be contained would have activity higher than Class C standards (Tian et al. 2017, 2018). For scenarios considering stress cracks (>2000 yr; Tian et al. 2017, 2018), the geomembrane was conservatively postulated to contain five stress cracks per hectare. Each stress crack was assumed to be 0.5 mm wide and 20 m long. The overburden pressure from the overlying cover soils was assumed to constrain movement of the geomembrane after stress cracking, thereby limiting the width of the opening in the geomembrane induced by stress cracking.

The saturated hydraulic conductivity of the GCL was assumed to be $1x10^{-10}$ m/s (as recommended in NUREG CR-7028 for conditions without specific data) or $1x10^{-11}$ m/s (based on recent exhumations of GCLs in composite barriers at sites in humid climates; Benson et al. 2010, Scalia et al. 2017), as described in Benson and Benavides (2018). The recommendation in NUREG CR-7028 (Benson et al. 2011) assumed that monovalent cations on the surface of the GCL would gradually be replaced by polyvalent cations, and that this exchange process would result in an increase in hydraulic conductivity due to a reduction in bound water associated with osmotic hydration (Jo et al. 2004). However, a recent study of an exhumed cover from Barnwell disposal facility in South Carolina, showed that GCLs hydrate and rapidly swell osmotically in humid climates, and that the water associated with this swelling process is strongly bound to the bentonite surface (Scalia et al. 2017). Consequently, even if cation exchange occurs, the hydraulic conductivity remains unchanged provided that the GCL does not dehydrate (Benson et al. 2010, Scalia and Benson 2011, Scalia et al. 2017). Due to the presence of the geomembrane, the GCL will not dehydrate, and low hydraulic conductivity will be maintained. Good contact ($C=0.21$ and $C_\infty=0.52$) was assumed between the GCL and geomembrane, which is typical in field conditions due to the uniformity of GCLs and the contribution of extruded bentonite in the interface to enhancing contact (Giroud 1997). The barrier thickness (t_g) was set at 8 mm, which is representative of a GCL thickness (geotextiles and bentonite) at the low stresses encountered in covers.

4. PERFORMANCE PREDICTION

4.1 Water Balance Above the Composite Barrier

Water balance quantities above the drainage layer in the ECC are shown in Fig. 6 for the typical year (1987) and the wettest ten-year period (1989-1998). These quantities were predicted by WinUNSAT-H and correspond to intact cover (no erosion gullies). Runoff is the smallest

fraction of the water balance, and evapotranspiration is the largest, which is expected for the South Carolina climate and cover profile. For all years, runoff was no more than 8% of the annual water balance, indicating that the hydraulic properties of the top soil layer are reasonable (Albright et al. 2010).

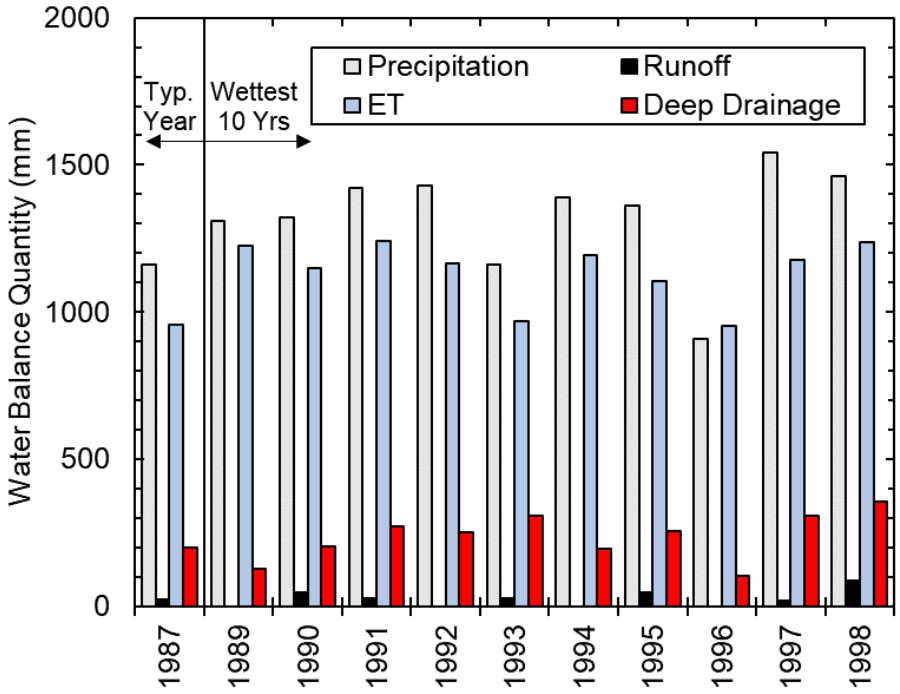

Fig. 6. Water balance above the drainage layer for the typical year and wettest 10-yr period.

Analyses were also conducted for cases where erosion gullies were assumed to reach the upper surface of the erosion barrier. This case is referred to as “anticipated erosion,” because the intent of the erosion barrier design is to halt erosion from progressing deeper into the ECC. For these analyses, WinUNSAT-H simulations were conducted without the upper backfill and topsoil layers and with reduced vegetation, representing the sparsely vegetated surface expected in the base of a gully. The precipitation input to WinUNSAT-H was increased for the anticipated erosion simulations to account for runoff from the intact portion of the cover entering the gully by adding the total volume of runoff from the intact cover per unit area of the gully bottom to the actual precipitation. Otherwise the inputs were identical to the input for an intact (no gully erosion)

cover profile. A “severe erosion” case was also considered corresponding to erosion of all earthen materials above the composite barrier. Simulations of the severe erosion case were not conducted with WinUNSAT-H because the earthen portion of the cover was eroded completed by the gully. This case is described in greater detail in the following section.

Annual deep drainage impinging on the drainage layer predicted by WinUNSAT-H is shown in Fig. 7 for intact cover and areas of the cover with “anticipated erosion.” The deep drainage rates in Fig. 7 for the intact cover are the same as those reported in Fig. 6. Deep drainage in the areas with anticipated erosion are typically lower than deep drainage in areas with intact cover, with a few exceptions. This occurs because the erosion barrier has lower saturated hydraulic conductivity than the topsoil, which promotes runoff and diminishes infiltration. The saturated hydraulic conductivity is lower, and will persist when the erosion barrier is exposed, because angular rock is the primary component of the erosion barrier.

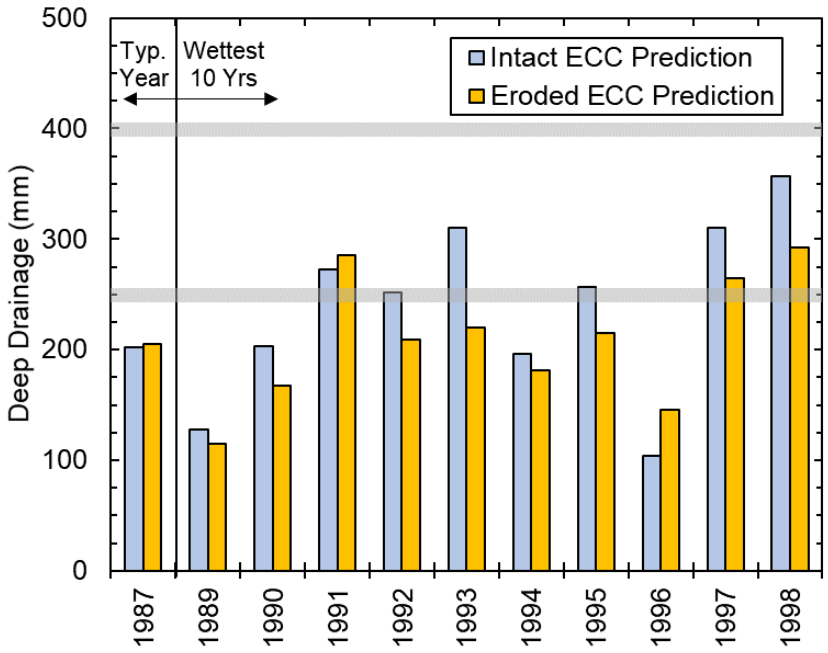

Fig. 7. Deep drainage in regions of intact cover and in areas with anticipated erosion gullies extending to surface of the erosion barrier for the typical year and wettest 10-yr period.

Deep drainage for the typical year is approximately 200 mm/yr. For the wettest 10-year period, the average deep drainage rate is approximately 250 mm/yr. Under a climate change scenario, this deep drainage rate could become as large as 400 mm/yr (60% higher). Under very severe climate change, the deep drainage rate might be as high as 650 mm/yr, as assumed by Benson and Benavides (2018) for the ECC over the SDF. Deep drainage rates of 250, 400, and 650 mm/yr were used as impingement rates for predicting percolation from the composite barrier for the ECC over HTF and FTF. Based on current predictions described here using the most up-to-date and accurate inputs, very severe conditions leading to 650 mm/yr of deep drainage are unlikely, but were included for comparison to Benson and Benavides (2018). The deep drainage rate of 400 mm/yr is comparable to the combined runoff and recharge rates reported by Hubbard and Emslie (1984) for lysimeter experiments at the Savannah River Site and regional recharge rates reported by Harder et al. (2007) and Reitz et al. (2017).

4.2 Percolation Rate from Composite Barrier

Percolation rates from the base of the composite barrier were predicted for the HTF and the FTF. The HTF has two sub-areas, the West Hill (herein HTF-W) and the East Hill (herein HTF-E) (Fig. 8). The HTF also has a smaller area corresponding to H Pump Pits 5 and 6 (*aka* HPP-5/6), which was not assessed. The FTF consists of a single area (Fig. 9). Each of the assessed areas (HTF-W, HTF-E, FTF) had similar slopes for the top deck and the drain layer, ranging from 3.9-4.7%. Differences in slope over this range had a negligible impact on the predicted percolation rates, and a slope of 4.0% (slope angle, $\beta = 2.3°$) was used for all calculations. Computations were made for the longest run for each enclosure (166 m for HTF-W, 141 m for HTF-E, and 139 m for FTF).

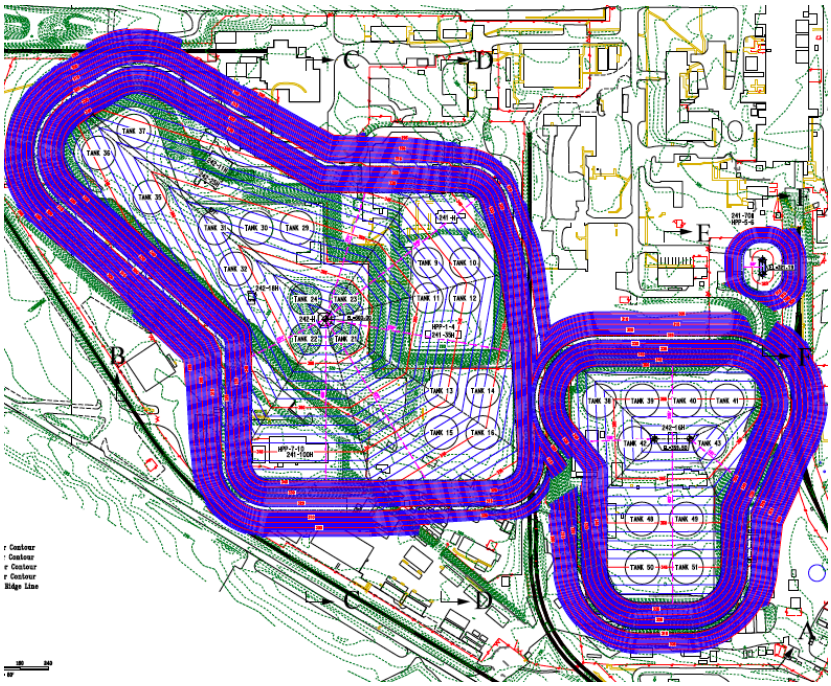

Fig. 8. Topographic representation of area for ECC over HTF. HTF-W (left) and HTF-E (right).

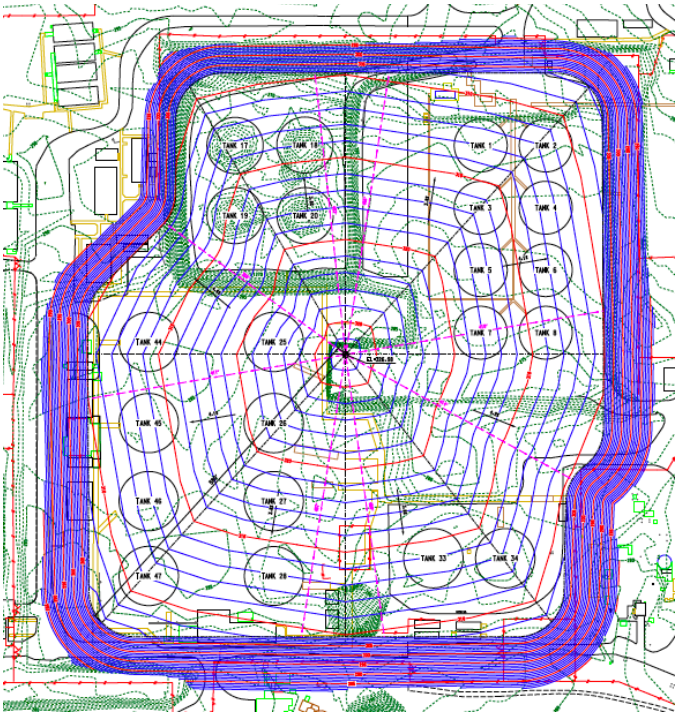

Fig. 9. Topographic representation of area for ECC over FTF.

Percolation rates were predicted for impingement rates of 250, 400, and 650 mm/yr. Computations were made for circular defects with diameters of 2 and 10 mm in the geomembrane, saturated hydraulic conductivity of the drainage layer of the $1x10^{-5}$, $1x10^{-4}$, or $5x10^{-4}$ m/s, and hydraulic conductivity of the GCL of $1x10^{-11}$ or $1x10^{-10}$ m/s. Similar inputs were used by Benson and Benavides (2018) for predicting percolation rates from the ECC over the SDF. Additional computations were made for long-term (> 2000 yr) scenarios where (i) stress cracks may form in the geomembrane and/or (ii) severe erosion occurs where all earthen material above the composite barrier are removed by an erosion gully. Percolation rates were not computed for the anticipated erosion case, as the impingement rate for areas within erosion gullies reaching the surface of the erosion barrier are generally comparable to impingement rates in areas of intact cover (Fig. 7). For severe gullies, the percolation rate in the gully area was assumed to be the deep drainage rate from the intact cover.

Percolation rates corresponding to the severe erosion case were computed as a weighted average based on the relative fractions of the cover that are intact and eroded. Gully dimensions were computed using Eq. 7 and the peak daily runoff predicted for the simulation period for the intact cover. For FTF and HTF-E, the largest contributing areas were nearly symmetrical, and were used for dimensioning gullies. For HTF-W, the two largest contributing areas were irregularly shaped and flow across these areas was unlikely to be concentrated into one channel; therefore, the third largest contributing area, which was nearly symmetrical, was used to determine the gully dimensions. Gullies for the severe erosion case had a bottom width of 7.6 m for the HTF-W and HTF-E and 6.7 m for the FTF. All gullies were assumed to have a rectangular cross-section with vertical side walls and a flat bottom.

4.2.1 Percolation Predictions for HTF

Percolation rates into the lower backfill for HTF-W and HTF-E are shown in Table 2 for an ECC with circular defects in the geomembrane, no stress cracks, and no severe erosion gullies.

For all conditions, percolation rates for HTF-W are equal to or higher than for HTF-E. When there are only 2 mm diameter circular defects in the geomembrane, the percolation rate should be less than 0.1 mm/yr until the stress crack resistance is exceeded (~2000 yr), regardless of the climatic condition, as long as the drain layer remains permeable (K_s = $5x10^{-4}$ m/s) and the hydraulic conductivity of the GCL remains low (K_s = $1x10^{-11}$ m/s) . After the antioxidants are depleted and oxidative degradation occurs, the circular defects in the geomembrane will become larger as broken bonds on the surface of the defect are attacked by oxidation. This scenario can be assessed using predictions for larger (10 mm) defects, which cause the percolation rate to increase by a factor of approximately 1.4. This increase in percolation rate may occur decades or centuries after the antioxidants are depleted given that the geomembrane is buried and will be under minimal tensile stress due to the mild slope of the ECC. Regardless, the percolation rate is still expected to be less than 0.1 mm/yr unless other components in the cover degrade in an unanticipated manner.

The most realistic percolation rate predictions correspond to the drainage layer maintaining a hydraulic conductivity of at least $5x10^{-4}$ m/s and the GCL maintaining a hydraulic conductivity of $1x10^{-11}$ m/s, assumptions that are consistent with near-term field observations and analogs from historical sites. If the hydraulic conductivity of the drainage layer decreases modestly, an unlikely but not completely unreasonable scenario, the percolation rate could increase just over 10 fold prior to antioxidants being depleted, and approximately 15 fold if the reduction in hydraulic conductivity of the drainage layer is concurrent with depletion of antioxidants in the geomembrane. However, the percolation rate would still remain less than 0.1 mm/yr unless the hydraulic conductivity of the GCL increases.

For the very wet condition corresponding to a long-term increase in annual precipitation due to severe climate change (impingement rate of 650 mm/yr, Benson and Benavides 2018),

Table 2. Summary of near- to long-term percolation rates predicted for HTF with five circular defects in the geomembrane, no stress cracks, and erosion no deeper than the erosion barrier.

Imping. Rate (mm/yr)	Drain Layer K_s (m/s)	Defect Diam. (mm)	GCL K_s (m/s)	Perc. Rate (mm/yr)		Comments
				HTF-W	HTF-E	
250	$5x10^{-4}$	2	$1x10^{-11}$	0.001	0.001	Most realistic near to mid-term
250	$1x10^{-4}$	2	$1x10^{-11}$	0.011	0.008	Reasonable mid-term
250	$1x10^{-4}$	2	$1x10^{-10}$	0.060	0.046	Reasonable mid-term with GCL per CR-7028
250	$1x10^{-5}$	2	$1x10^{-10}$	3.42	2.54	Highly unlikely case mid-term with GCL per CR-7028
250	$5x10^{-4}$	10	$1x10^{-11}$	0.001	0.001	Realistic long-term with
250	$1x10^{-4}$	10	$1x10^{-11}$	0.015	0.012	Reasonable long-term
250	$1x10^{-4}$	10	$1x10^{-10}$	0.083	0.064	Long-term with GCL per CR-7028
250	$1x10^{-5}$	10	$1x10^{-10}$	4.72	3.50	Long-term with severely affected drain and GCL per CR-7028; no stress cracks or gullies
400	$5x10^{-4}$	2	$1x10^{-11}$	0.002	0.002	Most realistic near to mid-term
400	$1x10^{-4}$	2	$1x10^{-11}$	0.024	0.018	Reasonable mid-term
400	$1x10^{-4}$	2	$1x10^{-10}$	0.133	0.100	Reasonable mid-term with GCL per CR-7028
400	$1x10^{-5}$	2	$1x10^{-10}$	8.07	5.97	Highly unlikely case mid-term with GCL per CR-7028
400	$5x10^{-4}$	10	$1x10^{-11}$	0.003	0.002	Realistic long-term
400	$1x10^{-4}$	10	$1x10^{-11}$	0.033	0.025	Reasonable long-term with
400	$1x10^{-4}$	10	$1x10^{-10}$	0.183	0.138	Long-term with GCL per CR-7028
400	$1x10^{-5}$	10	$1x10^{-10}$	11.1	8.24	Long-term with severely affected drain and GCL per CR-7028
650	$5x10^{-4}$	2	$1x10^{-11}$	0.004	0.003	Most realistic near to mid-term
650	$1x10^{-4}$	2	$1x10^{-11}$	0.056	0.042	Reasonable mid-term
650	$1x10^{-4}$	2	$1x10^{-10}$	0.306	0.230	Reasonable mid-term with GCL per CR-7028
650	$1x10^{-5}$	2	$1x10^{-10}$	19.7	14.5	Highly unlikely case upper bound with GCL per CR-7028
650	$5x10^{-4}$	10	$1x10^{-11}$	0.005	0.004	Realistic long-term
650	$1x10^{-4}$	10	$1x10^{-11}$	0.077	0.058	Reasonable long-term
650	$1x10^{-4}$	10	$1x10^{-10}$	0.423	0.317	Long-term with GCL per CR-7028
650	$1x10^{-5}$	10	$1x10^{-10}$	27.1	20.0	Long-term with severely affected drain, GCL per CR-7028

the long-term percolation rate is still predicted to be less than 0.1 mm/yr even when the antioxidants are depleted, as long as the hydraulic conductivity of the GCL does not increase. For all climate conditions, percolation rates in excess of 0.1 mm/yr are only realized when the hydraulic conductivity of the drainage layer is diminished or the hydraulic conductivity of the GCL increases. A long-term (>2000 yr) condition corresponding to the saturated hydraulic conductivity of the drainage layer diminishing to $1x10^{-5}$ m/s, larger circular defects in the geomembrane, and the GCL becoming 10 times more permeable (i.e., using the GCL hydraulic conductivity suggested in NUREG CR-7028) yields percolation rates from approximately 4.7 mm/yr (current climate) to 27 mm/yr (severe climate change). These scenarios are plausible, but highly unlikely.

Predictions of percolation rates into the lower backfill for HTF-W and HTF-E are shown in Table 3 for long-term scenarios (>2000 yr) that include 10 mm circular defects in the geomembrane in addition to stress cracks in the geomembrane and/or severe erosion gullies to the top of the composite barrier. These additional compromising features are unlikely due to relatively high overburden stress on the composite barrier and the mild slope of the cover, but are plausible under extreme long-term conditions. Even with the addition of stress cracks, the percolation rate remains below 0.1 mm/yr as long as the hydraulic conductivities of the drain layer and the GCL are unaffected. Formation of severe gullies has greater impact on the percolation rate, with percolation rates ranging from approximately 27 mm/yr to 104 mm/yr, depending on the climatic conditions, the enclosure geometry (HTF-W vs. HTF-E), and the condition of the drainage layer and GCL. The highest percolation rates are realized when severe gullies are combined with stress cracks, 10 mm circular defects, diminished hydraulic conductivity of the drain layer, and increased hydraulic conductivity of the GCL. Under these conditions, the percolation rate approaches 51 mm/yr for HTF-W and 43 mm/yr for HTF-E under current conditions, and approximately 171 mm/yr for HTF-W and 141 mm/yr for HTF-E for severe climate change.

Table 3. Summary of near- to long-term (>2000 yr) percolation rates predicted for HTF with five 10 mm circular defects in geomembrane per hectare, five stress cracks per hectare, and/or one severe gully per hectare.

Imp. Rate (mm/yr)	Drain Layer K_s (m/s)	GCL K_s (m/s)	Perc. Rate (mm/yr)		Comments
			W. Hill	E. Hill	
250	$5x10^{-4}$	$1x10^{-11}$	0.017	0.015	Stress cracks with unaffected drain layer and GCL, anticipated erosion or no gullies
250	$1x10^{-4}$	$1x10^{-10}$	0.859	0.691	Stress cracks with modestly affected drain layer and GCL, anticipated erosion or no gullies
250	$1x10^{-5}$	$1x10^{-10}$	23.6	18.4	Stress cracks with severely affected drain layer and modestly affected GCL, anticipated erosion or no gullies
250	$5x10^{-4}$	$1x10^{-11}$	30.7	26.7	Severe gullies with unaffected drain layer and GCL, no stress cracks
250	$1x10^{-4}$	$1x10^{-10}$	30.8	26.7	Severe gullies with modestly affected drain layer and GCL, no stress cracks
250	$1x10^{-5}$	$1x10^{-10}$	34.9	29.8	Severe gullies with severely affected drain layer and modestly affected GCL, no stress cracks
250	$5x10^{-4}$	$1x10^{-11}$	30.7	26.7	Severe gullies and stress cracks, with unaffected drain layer and GCL
250	$1x10^{-4}$	$1x10^{-10}$	31.5	27.3	Severe gullies and stress cracks, with modestly affected drain layer and GCL
250	$1x10^{-5}$	$1x10^{-10}$	51.4	43.1	Severe gullies and stress cracks, with severely affected drain layer and modestly affected GCL
400	$5x10^{-4}$	$1x10^{-11}$	0.029	0.024	Stress cracks with unaffected drain layer and GCL, anticipated erosion or no gullies
400	$1x10^{-4}$	$1x10^{-10}$	1.63	1.30	Stress cracks with modestly affected drain layer and GCL, anticipated erosion or no gullies
400	$1x10^{-5}$	$1x10^{-10}$	48.6	37.7	Stress cracks with severely affected drain layer and modestly affected GCL, anticipated erosion or no gullies.
400	$5x10^{-4}$	$1x10^{-11}$	49.2	42.7	Severe gullies with unaffected drain layer and GCL, no stress cracks.
400	$1x10^{-4}$	$1x10^{-10}$	49.3	42.8	Severe gullies with modestly affected drain layer and GCL, no stress cracks
400	$1x10^{-5}$	$1x10^{-10}$	58.9	50.1	Severe gullies with severely affected drain layer and modestly affected GCL, no stress cracks
400	$5x10^{-4}$	$1x10^{-11}$	49.2	42.7	Severe gullies and stress cracks, with unaffected drain layer and GCL
400	$1x10^{-4}$	$1x10^{-10}$	50.6	43.9	Severe gullies and stress cracks, with modestly affected drain layer and GCL
400	$1x10^{-5}$	$1x10^{-10}$	91.7	76.3	Severe gullies and stress cracks, with severely affected drain layer and modestly affected GCL
650	$5x10^{-4}$	$1x10^{-11}$	0.052	0.043	Stress cracks with unaffected drain layer and GCL, anticipated erosion or no gullies
650	$1x10^{-4}$	$1x10^{-10}$	3.23	2.55	Stress cracks with modestly affected drain layer and GCL, anticipated erosion or no gullies
650	$1x10^{-5}$	$1x10^{-10}$	104	80.0	Stress cracks with severely affected drain layer and modestly affected GCL, anticipated erosion or no gullies
650	$5x10^{-4}$	$1x10^{-11}$	79.9	69.4	Severe gullies with unaffected drain layer and GCL, no stress cracks
650	$1x10^{-4}$	$1x10^{-10}$	80.2	69.7	Severe gullies with modestly affected drain layer and GCL, no stress cracks
650	$1x10^{-5}$	$1x10^{-10}$	104	87.3	Severe gullies with severely affected drain layer and modestly affected GCL, no stress cracks
650	$5x10^{-4}$	$1x10^{-11}$	79.9	69.4	Severe gullies and stress cracks, with unaffected drain layer and GCL
650	$1x10^{-4}$	$1x10^{-10}$	82.7	71.7	Severe gullies and stress cracks, with modestly affected drain layer and GCL
650	$1x10^{-5}$	$1x10^{-10}$	171	141	Severe gullies and stress cracks, with severely affected drain layer and modestly affected GCL

4.2.2 Percolation Predictions for FTF

Predictions of percolation rates into the lower backfill for FTF are shown in Table 4 for an ECC with circular defects in the geomembrane, no stress cracks, and no erosion or anticipated erosion gullies. Similar to the predictions for HTF, the percolation rate for FTF is less than 0.1 mm/yr for all climatic conditions unless the hydraulic conductivity of the drain layer is diminished and/or the hydraulic conductivity of the GCL increases. The most unfavorable long-term (>2000 yr) conditions of the drain layer and GCL result in percolation predictions ranging from approximately 3.4 mm/yr to 20 mm/yr.

Percolation rates into the lower backfill predicted for FTF are shown in Table 5 for long-term scenarios (>2000 yr) that include 10 mm circular defects in the geomembrane, stress cracks in the geomembrane, and/or severe erosion gullies. Similar to HTF, these features result in percolation rates as high as 38 mm/yr (current climate) to 127 mm/yr (severe climate change). As with HTF, these scenarios are plausible but unlikely. Severe gullies have the greatest impact on percolation rate. Thus, efficacy of the erosion barrier is critically important.

5. RECOMMENDATIONS

Percolation rates recommended for the performance assessment are summarized in Table 6 for HTF and Table 7 for FTF for long-term average climatic conditions and for very wet climatic conditions that might be encountered in response to potential climate change. A lower bound of 0.1 mm/yr is cited here, rather than a specific percolation rate, because 0.1 mm/yr is the resolution with which percolation rates can be measured in the field (Benson et al. 2001). The recommendations correspond to realistic and expected conditions, unlikely upper bound conditions (<5% likelihood), and highly unlikely severe conditions (<1% likelihood).

Table 4. Summary of near- to long-term percolation rates predicted for FTF with five circular defects in the geomembrane, no stress cracks, and erosion no deeper than the erosion barrier.

Imping. Rate (mm/yr)	Drain Layer K_s (m/s)	Defect Diam. (mm)	GCL K_s (m/s)	Perc. Rate (mm/yr)	Comments
250	$5x10^{-4}$	2	$1x10^{-11}$	0.001	Most realistic near to mid-term
250	$1x10^{-4}$	2	$1x10^{-11}$	0.008	Reasonable mid-term
250	$1x10^{-4}$	2	$1x10^{-10}$	0.045	Reasonable mid-term with GCL per CR-7028
250	$1x10^{-5}$	2	$1x10^{-10}$	2.48	Highly unlikely case mid-term with GCL per CR-7028
250	$5x10^{-4}$	10	$1x10^{-11}$	0.001	Realistic long-term
250	$1x10^{-4}$	10	$1x10^{-11}$	0.011	Realistic long-term
250	$1x10^{-4}$	10	$1x10^{-10}$	0.063	Long-term with GCL per CR-7028
250	$1x10^{-5}$	10	$1x10^{-10}$	3.42	Long-term highly unlikely case with severely affected drain and GCL per CR-7028
400	$5x10^{-4}$	2	$1x10^{-11}$	0.002	Most realistic near to mid-term
400	$1x10^{-4}$	2	$1x10^{-11}$	0.018	Reasonable mid-term
400	$1x10^{-4}$	2	$1x10^{-10}$	0.098	Reasonable mid-term with GCL per CR-7028
400	$1x10^{-5}$	2	$1x10^{-10}$	5.83	Highly unlikely case mid-term with GCL per CR-7028
400	$5x10^{-4}$	10	$1x10^{-11}$	0.002	Realistic long-term
400	$1x10^{-4}$	10	$1x10^{-11}$	0.025	Realistic long-term
400	$1x10^{-4}$	10	$1x10^{-10}$	0.135	Long-term with GCL per CR-7028
400	$1x10^{-5}$	10	$1x10^{-10}$	8.04	Long-term highly unlikely case with severely affected drain, GCL per CR-7028
650	$5x10^{-4}$	2	$1x10^{-11}$	0.003	Most realistic near to mid-term
650	$1x10^{-4}$	2	$1x10^{-11}$	0.041	Reasonable mid-term
650	$1x10^{-4}$	2	$1x10^{-10}$	0.225	Reasonable mid-term with GCL per CR-7028
650	$1x10^{-5}$	2	$1x10^{-10}$	14.2	Highly unlikely case upper bound with GCL per CR-7028
650	$5x10^{-4}$	10	$1x10^{-11}$	0.004	Realistic long-term
650	$1x10^{-4}$	10	$1x10^{-11}$	0.056	Realistic long-term
650	$1x10^{-4}$	10	$1x10^{-10}$	0.310	Long-term with GCL per CR-7028
650	$1x10^{-5}$	10	$1x10^{-10}$	19.6	Long-term with severely affected drain and GCL per CR-7028

Table 5. Summary of near- to long-term (>2000 yr) percolation rates predicted for FTF with five 10 mm circular defects in geomembrane per hectare, five stress cracks per hectare, and/or one severe gully per hectare.

Imping. Rate (mm/yr)	Drain Layer K_s (m/s)	GCL K_s (m/s)	Perc. Rate (mm/yr)	Condition
250	$5x10^{-4}$	$1x10^{-11}$	0.014	Stress cracks, unaffected drain layer & GCL, anticipated erosion or no gullies
250	$1x10^{-4}$	$1x10^{-10}$	0.679	Stress cracks, modestly affected drain layer & GCL, anticipated erosion or no gullies
250	$1x10^{-5}$	$1x10^{-10}$	18.0	Stress cracks, severely affected drain layer & modestly affected GCL, anticipated erosion or no gullies. Highly unlikely case.
250	$5x10^{-4}$	$1x10^{-11}$	21.2	Severe gullies, unaffected drain layer & GCL, no stress cracks
250	$1x10^{-4}$	$1x10^{-10}$	21.3	Severe gullies, modestly affected drain layer & GCL, no stress cracks
250	$1x10^{-5}$	$1x10^{-10}$	24.4	Severe gullies, severely affected drain layer & modestly affected GCL, no stress cracks. Highly unlikely case.
250	$5x10^{-4}$	$1x10^{-11}$	21.2	Severe gullies & stress cracks, unaffected drain layer & GCL
250	$1x10^{-4}$	$1x10^{-10}$	21.8	Severe gullies & stress cracks, modestly affected drain layer & GCL
250	$1x10^{-5}$	$1x10^{-10}$	37.7	Severe gullies & stress cracks, severely affected drain layer & modestly affected GCL. Highly unlikely case.
400	$5x10^{-4}$	$1x10^{-11}$	0.024	Stress cracks with unaffected drain layer & GCL, anticipated erosion or no gullies
400	$1x10^{-4}$	$1x10^{-10}$	1.27	Stress cracks, modestly affected drain layer & GCL, anticipated erosion or no gullies
400	$1x10^{-5}$	$1x10^{-10}$	36.9	Stress cracks, severely affected drain layer & modestly affected GCL, anticipated erosion or no gullies. Highly unlikely case.
400	$5x10^{-4}$	$1x10^{-11}$	34.0	Severe gullies, unaffected drain layer & GCL, no stress cracks
400	$1x10^{-4}$	$1x10^{-10}$	34.1	Severe gullies, modestly affected drain layer & GCL, no stress cracks
400	$1x10^{-5}$	$1x10^{-10}$	41.3	Severe gullies, severely affected drain layer & modestly affected GCL, no stress cracks
400	$5x10^{-4}$	$1x10^{-11}$	34.0	Severe gullies & stress cracks, unaffected drain layer & GCL
400	$1x10^{-4}$	$1x10^{-10}$	35.1	Severe gullies & stress cracks, modestly affected drain layer & GCL
400	$1x10^{-5}$	$1x10^{-10}$	67.7	Severe gullies & stress cracks, severely affected drain layer & modestly affected GCL. Highly unlikely case.
650	$5x10^{-4}$	$1x10^{-11}$	0.042	Stress cracks, unaffected drain layer & GCL, anticipated erosion or no gullies
650	$1x10^{-4}$	$1x10^{-10}$	2.50	Stress cracks, modestly affected drain layer & GCL, anticipated erosion or no gullies
650	$1x10^{-5}$	$1x10^{-10}$	78.4	Stress cracks, severely affected drain layer & modestly affected GCL, anticipated erosion or no gullies. Highly unlikely case.
650	$5x10^{-4}$	$1x10^{-11}$	55.2	Severe gullies, unaffected drain layer & GCL, no stress cracks
650	$1x10^{-4}$	$1x10^{-10}$	55.5	Severe gullies, modestly affected drain layer & GCL, no stress cracks
650	$1x10^{-5}$	$1x10^{-10}$	73.1	Severe gullies, severely affected drain layer & modestly affected GCL, no stress cracks. Highly unlikely case.
650	$5x10^{-4}$	$1x10^{-11}$	55.2	Severe gullies & stress cracks, unaffected drain layer & GCL
650	$1x10^{-4}$	$1x10^{-10}$	57.5	Severe gullies & stress cracks, modestly affected drain layer & GCL
650	$1x10^{-5}$	$1x10^{-10}$	127	Severe gullies & stress cracks, severely affected drain layer & modestly affected GCL. Highly unlikely case.

Table 6. Summary of recommended percolation rates for HTF for various scenarios.

Time Frame (yr)	Climatic Condition	Drainage Layer Condition	Geomembrane State	Perc. Rate (mm/yr)		Comments
				HTF-W	HTF-E	
0-2000	Current	Realistic & expected	Antioxidants present	0.1	0.1	Realistic & expected
1000-2000	Current	Less permeable	Antioxidants present	0.1	0.1	Reasonable mid-term upper bound
1000-2000	Current	Less permeable	Antioxidants present	0.1	0.1	Reasonable mid-term with GCL per CR-7028
1000-2000	Current	Much less permeable	Antioxidants present	3.4	2.5	Highly unlikely case with GCL per CR-7028
>2000	Current	Less permeable	Antioxidants depleted	0.1	0.1	Realistic long-term
>2000	Current	Less permeable	Antioxidants depleted	0.1	0.1	Long-term highly unlikely case with GCL per CR-7028
>2000	Current	Much less permeable	Antioxidants depleted	4.7	3.5	Long-term highly unlikely case without stress cracks or severe gullies
>2000	Current	Much less permeable	Antioxidants depleted, stress cracks	24	18	Long-term highly unlikely case with stress cracks
>2000	Current	Much less permeable	Antioxidants depleted, degraded at gully bottom	35	30	Long-term highly unlikely case with severe gullies
>2000	Current	Much less permeable	Antioxidants depleted, stress cracks, degraded at gully bottom	51	43	Long-term highly unlikely case
0-2000	Anticipated change	Realistic & expected	Antioxidants present	0.1	0.1	Realistic & expected
1000-2000	Anticipated change	Less permeable	Antioxidants present	0.1	0.1	Reasonable mid-term upper bound
1000-2000	Anticipated change	Less permeable	Antioxidants present	0.1	0.1	Reasonable mid-term with GCL per CR-7028
1000-2000	Anticipated change	Much less permeable	Antioxidants present	8.1	6.0	Highly unlikely case with GCL per CR-7028
>2000	Anticipated change	Less permeable	Antioxidants depleted	0.1	0.1	Realistic long-term
>2000	Anticipated change	Less permeable	Antioxidants depleted	0.2	0.1	Long-term with GCL per CR-7028
>2000	Anticipated change	Much less permeable	Antioxidants depleted	11	8.2	Long-term highly unlikely case without stress cracks or severe gullies

Table 6. Summary of recommended percolation rates for HTF for various scenarios (con't.).

Time Frame (yr)	Climatic Condition	Drainage Layer Condition	Geomembrane State	Perc. Rate (mm/yr)		Comments
				HTF-W	HTF-E	
>2000	Anticipated change	Much less permeable	Antioxidants depleted, stress cracks	49	38	Long-term highly unlikely case with stress cracks
>2000	Anticipated change	Much less permeable	Antioxidants depleted, degraded at gully bottom	59	50	Long-term highly unlikely case with severe gullies
>2000	Anticipated change	Much less permeable	Antioxidants depleted, stress cracks, degraded at gully bottom	92	76	Long-term highly unlikely case
0-2000	Severe change	Realistic & expected	Antioxidants present	0.1	0.1	Realistic & expected
1000-2000	Severe change	Less permeable	Antioxidants present	0.1	0.1	Reasonable mid-term upper bound
1000-2000	Severe change	Less permeable	Antioxidants present	0.3	0.2	Reasonable mid-term with GCL per CR-7028
1000-2000	Severe change	Much less permeable	Antioxidants present	20	15	Highly unlikely case with GCL per CR-7028
>2000	Severe change	Less permeable	Antioxidants depleted	0.1	0.1	Realistic long-term
>2000	Severe change	Less permeable	Antioxidants depleted	0.4	0.3	Long-term with GCL per CR-7028
>2000	Severe change	Much less permeable	Antioxidants depleted	27	20	Long-term highly unlikely case without stress cracks or severe gullies
>2000	Severe change	Much less permeable	Antioxidants depleted, stress cracks	104	80	Long-term highly unlikely case with stress cracks
>2000	Severe change	Much less permeable	Antioxidants depleted, degraded at gully bottom	104	87	Long-term highly unlikely case with severe gullies
>2000	Severe change	Much less permeable	Antioxidants depleted, stress cracks, degraded at gully bottom	171	141	Long-term highly unlikely case

Table 7. Summary of recommended percolation rates for FTF for various scenarios.

Time Frame (yr)	Climate Condition	Drainage Layer Condition	Geomembrane State	Perc. Rate (mm/yr)	Comments
0-2000	Current	Realistic & expected	Antioxidants present	0.1	Realistic & expected
1000-2000	Current	Less permeable	Antioxidants present	0.1	Reasonable mid-term upper bound
1000-2000	Current	Less permeable	Antioxidants present	0.1	Reasonable mid-term with GCL per CR-7028
1000-2000	Current	Much less permeable	Antioxidants present	2.5	Highly unlikely case with GCL per CR-7028
>2000	Current	Less permeable	Antioxidants depleted	0.1	Realistic long-term
>2000	Current	Less permeable	Antioxidants depleted	0.1	Long-term, GCL per CR-7028
>2000	Current	Much less permeable	Antioxidants depleted	3.4	Long-term, highly unlikely case with no stress cracks or severe gullies
>2000	Current	Much less permeable	Antioxidants depleted, stress cracks	18	Long-term, highly unlikely case with stress cracks
>2000	Current	Much less permeable	Antioxidants depleted, degraded at gully bottom	24	Long-term, highly unlikely case with severe gullies
>2000	Current	Much less permeable	Antioxidants depleted, stress cracks, degraded at gully bottom	38	Long-term highly unlikely case
0-2000	Anticipated change	Realistic & expected	Antioxidants present	0.1	Realistic & expected
1000-2000	Anticipated change	Less permeable	Antioxidants present	0.1	Reasonable mid-term upper bound
1000-2000	Anticipated change	Less permeable	Antioxidants present	0.1	Reasonable mid-term with GCL per CR-7028
1000-2000	Anticipated change	Much less permeable	Antioxidants present	5.8	Highly unlikely case with GCL per CR-7028
>2000	Anticipated change	Less permeable	Antioxidants depleted	0.1	Realistic long-term

Table 7. Summary of recommended percolation rates for FTF for various scenarios (con't.).

Time Frame (yr)	Climate Condition	Drainage Layer Condition	Geomembrane State	Perc. Rate (mm/yr)	Comments
>2000	Anticipated change	Less permeable	Antioxidants depleted	0.1	Long-term, GCL per CR-7028
>2000	Anticipated change	Much less permeable	Antioxidants depleted	8.0	Long-term, highly unlikely case without stress cracks or severe gullies
>2000	Anticipated change	Much less permeable	Antioxidants depleted, stress cracks	37	Long-term, highly unlikely case with stress cracks
>2000	Anticipated change	Much less permeable	Antioxidants depleted, degraded at gully bottom	41	Long-term, highly unlikely case with severe gullies
>2000	Anticipated change	Much less permeable	Antioxidants depleted, stress cracks, degraded at gully bottom	68	Long-term highly unlikely case
0-2000	Severe change	Realistic & expected	Antioxidants present	0.1	Realistic & expected
1000-2000	Severe change	Less permeable	Antioxidants present	0.1	Reasonable mid-term upper bound
1000-2000	Severe change	Less permeable	Antioxidants present	0.2	Reasonable mid-term with GCL per CR-7028
1000-2000	Severe change	Much less permeable	Antioxidants present	14	Highly unlikely case with GCL per CR-7028
>2000	Severe change	Less permeable	Antioxidants depleted	0.1	Realistic long-term
>2000	Severe change	Less permeable	Antioxidants depleted	0.3	Long-term, GCL per CR-7028
>2000	Severe change	Much less permeable	Antioxidants depleted	20	Long-term, highly unlikely case without stress cracks or severe gullies
>2000	Severe change	Much less permeable	Antioxidants depleted, stress cracks	78	Long-term, highly unlikely case with stress cracks
>2000	Severe change	Much less permeable	Antioxidants depleted, degraded at gully bottom	73	Long-term, highly unlikely case with severe gullies
>2000	Severe change	Much less permeable	Antioxidants depleted, stress cracks, degraded at gully bottom	127	Long-term highly unlikely case

6. QUALITY ASSURANCE

Quality assurance for this study was conducted in general accordance with the "UVA Quality Assurance Document for Research Conducted in Support of SRR" (6 March 2017). S. Gustitus was responsible for the computations in this study. C. Benson was the primary checker. N. Chen was the secondary checker.

7. REFERENCES

Electronic copies of the references can be found here: https://tinyurl.com/ybn8qyk7

Albright, W., Benson, C., Gee, G., Roesler, A., Abichou, T., Apiwantragoon, P., Lyles, B., and Rock, S. (2004), Field Water Balance of Landfill Final Covers. *J. Environmental Quality*, 33(6), 2317-2332.

Albright, W., Benson, C., Gee, G., Abichou, T., Tyler, S., Rock, S. (2006), Field Performance of a Compacted Clay Landfill Final Cover at A Humid Site, *J. Geotech. Geoenvironmental Eng.,* 132(11), 1393-1403.

Albright, W., Benson, C., and Waugh, W. (2010), *Water Balance Covers for Waste Containment: Principles and Practice*, ASCE Press, Reston, VA, 158 p.

Allen, R., Pereira, L., Raes, D., and Smith, M. (1998). Crop Evapotranspiration-Guidelines for Computing Crop Water Requirements. FAO Irrigation and Drainage Paper 56, Food and Agricultural Organization of the United Nations, Rome.

Apiwantragoon, P., Benson, C., and Albright, W. (2014), Field Hydrology of Water Balance Covers for Waste Containment, *J. Geotech. Geoenvironmental Eng.,* 04014101-1-20.

Bareither, C. and Benson, C. (2013), Evaluation of Bouwer-Rice Large-Particle Correction Procedure for Soil Water Characteristic Curves, *Geotechnical Testing J.*, 36(5), 680-694.

Bareither, C., Foley, J., and Benson, C. (2015), Using Surrogate Meteorological Data to Predict the Hydrology of a Water Balance Cover, *J. Environmental Engineering*, *Geotech. and Geoenvironmental Eng.,* 04015092-1-16.

Benson, C. (2001), Waste Containment: Strategies and Performance, *Australian Geomechanics*, 36(4), 1-25.

Benson, C. (2006), Numerical Modeling in Geoenvironmental Practice, *Geo-Strata*, Aug. 2006, 16-19.

Benson, C. (2010), Predictions in Geoenvironmental Engineering: Recommendations for Reliable Predictive Modeling, *GeoFlorida 2010, Advances in Analysis, Modeling, and Design*, Geotechnical Special Publication No. 199, D. Fratta, A. Puppula, and B. Muhunthan, eds., ASCE, Reston, VA, 1-13.

Benson, C., Abichou, T., Albright, W., Gee, G., and Roesler, A. (2001), Field Evaluation of Alternative Earthen Final Covers, *International J. Phytoremediation*, 3(1), 1-21.

Benson, C., Albright, W., Fratta, D., Tinjum, J., Kucukkirca, E., Lee, S., Scalia, J., Schlicht, P., and Wang, X. (2011), Engineered Covers for Waste Containment: Changes in Engineering Properties & Implications for Long-Term Performance Assessment, NUREG CR-7028, Office of Research, US Nuclear Regulatory Commission, Washington, DC.

Benson, C. and Bareither, C. (2012), Designing Water Balance Covers for Sustainable Waste Containment: Transitioning State-of-the-Art to State-of-the-Practice, *State of the Art and Practice in Geotechnical Engineering, Keynote Lectures from GeoCongress 2012, GSP No. 226,* K. Rollins and D. Zekkos, eds., ASCE, Reston VA, 1-32.

Benson, C., Bohnhoff, G., Apiwantragoon, P., Ogorzalek, A., Shackelford, C., and Albright, W. (2004), Comparison of Model Predictions and Field Data for an ET Cover, *Tailings and Mine Waste '04*, Balkema, Leiden, Netherlands, 137-142.

Benson, C. and Benavides, J. (2018), Predicting Long-Term Percolation from the SDF Closure Cap, Report No. GENV-18-05, School of Engineering, University of Virginia.

Benson, C., Kucukkirca, I., and Scalia, J. (2010), Properties of Geosynthetics Exhumed from the Final Cover at a Solid Waste Landfill, *J. Geotextiles and Geomembranes*, 28, 536-546.

Benson, C., Sawangsuriya, A., Trzebiatowski, B., and Albright, W. (2007), Post-Construction Changes in the Hydraulic Properties of Water Balance Cover Soils, *J. Geotech. Geoenvironmental Eng.,* 133(4), 349-359.

Bjornstad, B. and Teel, S. (1993), Natural Analog Study of Engineered Protective Barriers at the Hanford Site, PNL-8840, Pacific Northwest Laboratory, Richland, WA.

Bohnhoff, G., Ogorzalek, A., Benson, C., Shackelford, C., and Apiwantragoon, P. (2009), Field Data and Water-Balance Predictions for a Monolithic Cover in a Semiarid Climate, *J. Geotech. Geoenvironmental Eng.*, 135(3), 333-348.

Chadwick, D., Ankeny, M., Greer, L., Mackey, C., and McClain, M. (1999), Field Test of Potential RCRA-Equivalent Covers at the Rocky Mountain Arsenal, *Proc. SWANA 4th Annual Landfill Symp.*, SWANA Publication No. GR-LM-0004, Silver Spring, MD, 12-33.

Carter, L., Jones, J., Berry, L., Burkett, V., Murley, J., Obeysekera, J., Schramm, P., and D. Wear, D. (2014), Ch. 17: Southeast and the Caribbean. *Climate Change Impacts in the United States: The Third National Climate Assessment*, J. M. Melillo, Terese (T.C.) Richmond, and G. W. Yohe, Eds., U.S. Global Change Research Program, 396-417.

Doorenbos, J. and Pruitt, W. (1977), Guidelines for Predicting Crop Agriculture Requirements. *FAO Irrigation Paper No. 24, 2nd Edition*, Food and Agricultural Organization of the United Nations, Rome, Italy.

Fayer, M. (2000), UNSAT-H Version 3.0: Unsaturated Soil Water and Heat Flow Model - Theory, User Manual, and Examples. PNNL-13249, Pacific Northwest Laboratories, Richland, WA,

USA.

Fayer, M. and Gee, G. (1997), Hydrologic Model Tests for Landfill Covers Using Field Data, *Proc. Landfill Capping in the Semi-Arid West: Problems, Perspectives, and Solutions*, Environmental Science and Research Foundation, Idaho Falls, ID, 53-68.

Fayer, M., Rockhold, M., and Campbell, M. (1992), Hydrologic Modeling of Protective Barriers: Comparison of Field Data and Simulation Results, *Soil Sci. Soc. of Am. J.*, 56, 690-700.

Feddes, R., and Zaradny, H. (1978), Model for Simulating Soil Water Content Considering Evapotranspiration, *J. Hydrology*, 37, 393-397.

Foose, G., Benson, C., and Edil, T. (2001), Predicting Leakage Through Composite Landfill Liners, *J. Geotech. and Geoenviron. Eng.,* 127(6), 510-520.

Gelaro, R., McCarty, W., Suárez, M.J., Todling, R., Molod, A., Takacs, L., Randles, C., Darmenov, A., Bosilovich, M., Reichle, R. and Wargan, K. (2017). The modern-era retrospective analysis for research and applications, version 2 (MERRA-2). *Journal of Climate*, 30(14), 5419-5454.

Giroud, J. (1997), Equations for Calculating the Rate of Liquid Migration Through Composite Liners due to Geomembrane Defects, *Geosynthetics International*, 4(3-4) 335-348.

Giroud, J. and Bonaparte, R. (1989), Leakage Through Liners Constructed with Geomembranes – Part I. Geomembrane Liners, *J. Geotextiles and Geomembranes*, 8, 27-67.

Giroud, J., Zhao, A., Tomlinson, H., and Zornberg, J. (2004), Liquid Flow Equations for Drainage Systems Composited of Two Layers Including a Geocomposite, *Geosynthetics International*, 11(1) 43-58.

Harder, S., Amatya, D., Callahan, T., Trettin, C., and Hakkila, J. (2007), Hydrology and Water Budget for a Forested Atlantic Coastal Plain Watershed, South Carolina, *J. of the American Water Works Association*, 43(3), 563-575.

Hubbard, J. and Emslie, R. (1984), Water Budget for SRP Burial Ground Area, DPST-83-742, 19 March 1984.

Hudson, M. and Barnes, G. (1991), Yoshinogari: A Yayoi Settlement in Northern Kyushu, *Monumenta Nipponica*, 46(2), 211-235.

Jo, H., Benson, C., and Edil, T. (2004), Hydraulic Conductivity and Cation Exchange in Non-Prehydrated and Prehydrated Bentonite Permeated with Weak Inorganic Salt Solutions, *Clays and Clay Minerals*, 52(6), 661-679.

Jones, W. and Phifer, M. (2008), Saltstone Disposal Facility Closure Cap Concept and Infiltration Estimates, WSRC-STI-2008-00244, Savannah River National Laboratory, Aiken, SC.

Khire, M., Benson, C., and Bosscher, P. (1997), Water Balance Modeling of Earthen Final Covers, *J. Geotech. Geoenvironmental Eng.*, 123(8), 744-754.

Khire, M., Benson, C., and Bosscher, P. (1999), Field Data from a Capillary Barrier in a Semi-Arid Climate and Model Predictions with UNSAT-H, *J. Geotech. Geoenvironmental Eng.,* 125(6), 518-528.

Koerner, R. (2005), *Designing with Geosynthetics*, Pearson Prentice Hall, Upper Saddle River, NJ.

López-Serrano, F., Landete-Castillejos, T., Martinez-Millán, T., and Cerro-Barja, A. (2000), LAI Estimation of Natural Pine Forest using a Non-Standard Sampling Technique, *Agricultural and Forest Meteorology*, 101, 95–111.

Ogorzalek, A., Bohnhoff, G., Shackelford, C., Benson, C., and Apiwantragoon, P. (2008), Comparison of Field Data and Water-Balance Predictions for a Capillary Barrier Cover. *J. Geotech. and Geoenvironmental Eng.*, 134(4), 470-486.

Onitsuka, K., Lu, J., Tang, X., Hara, Y., and Kai, D. (2003), Geotechnical Characteristics and Construction Methods of Voshinogari Fun-Kyu Tomb in Japan and Tu-Dun Tombs in China. *J. Geotech. Engr.,* (736), 1-17.

Reitz, M., Sanford, W., Senay, G., and Cazenas, J. (2017), Annual Estimates of Recharge, Quick-Flow Runoff, and Evapotranspiration for the Contiguous US Using Empirical Regression Equations, *J. of the American Water Works Association*, 53(4), 961-983.

Roesler, A., Benson, C., and Albright, W. (2002), Field Hydrology and Model Predictions for Final Covers in the Alternative Assessment Program. Geo Engineering Report No. 02-08, University of Wisconsin-Madison.

Scalia, J. and Benson, C. (2011), Hydraulic Conductivity of Geosynthetic Clay Liners Exhumed from Landfill Final Covers with Composite Barriers, *J. Geotech. Geoenvironmental Eng.,* 137(1), 1-13.

Scalia, J., Benson, C., Albright, W., Smith, B., and Wang, X. (2017), Properties of Barrier Components in a Composite Cover after 14 Years of Service and Differential Settlement, *J. Geotech. and Geoenvironmental Eng.,* 04017055-1-11.

Scanlon, B., Christman, M., Reedy, R., Porro, I., Šimůnek, J., and Flerchinger, G. (2002), Intercode Comparisons for Simulating Water Balance of Surficial Sediments in Semiarid Regions, *Water Resources Research*, 38(12), 59-1 - 59-16.

Sidorchuk, A. (1999). Dynamic and static models of gully erosion. *Catena*, 37(3-4), 401-414.

Tian, K. and Benson, C. (2018), Radiation Dose and Antioxidant Depletion in HDPE Geomembranes, *J. Geotextiles and Geomembranes*, 46, 426-435.

Tian, K., Benson, C., and Likos, W. (2016), Hydraulic Conductivity of Geosynthetic Clay Liners to Low-Level Radioactive Waste Leachate, *J. Geotech. and Geoenvironmental Eng.,* 04016037, 1-12.

Tian, K., Benson, C., Tinjum, J. and Edil, T. (2017), Antioxidant Depletion and Service Life Prediction for HDPE Geomembranes Exposed to Low-Level Radioactive Waste Leachate, *J. Geotech. Geoenvironmental Eng.,* 04017011-1-11.

van Genuchten, M. (1980), A Closed-form Equation for Predicting the Hydraulic Conductivity of Unsaturated Soils. Soil Science Society of America Journal, 44(5), 892-895.

Walsh, J., Wuebbles, D., Hayhoe, K., Kossin, J. Kunkel, K., Stephens, G., Thorne, P., Vose, R., Wehner, M., Willis, J., Anderson, D., Doney, S., Feely, R., Hennon, P., Kharin, V., Knutson, T., Landerer, F., Lenton, T., Kennedy, J., and R. Somerville, R. (2014). Ch. 2: Our Changing Climate. *Climate Change Impacts in the United States: The Third National Climate Assessment*, J. Melillo, T. Richmond, and G. Yohe, Eds., U.S. Global Change Research Program, 19-67.

Zhaoming, Z., Guojin H., Wang, X., and Jiang, H. (2011), Leaf Area Index Estimation of Bamboo Forest in Fujian Province Based on IRS P6 LISS 3 Imagery*, International Journal of Remote Sensing*, 32(19), 5365-5379.